A Multifunctional Polarization Converter Base on the Solid-State Plasma Metasurface

Yu-Peng Li, Hai-Feng Zhang, Tong Yang, Tang-Yi Sun, and Li Zeng

***Abstract*— A novel multifunctional polarization converter (PC) based on the solid-state plasma (SSP) is proposed, which can switch two functions and adjust the working band. By energizing different parts of SSP resonators, the presented PC can accomplish three different operating states. In the state 1, this PC can operate in 6.12-9.50 GHz and the relative bandwidth (RB) is 43.3%, which can achieve the aim of the linear-to-circular polarization conversion (LCPC). In the state 2, the cross-polarization conversion (CPC) can be achieved in 4.62-8.34 GHz (the RB is 57.4%). Besides, in the state 3, such a PC can be implemented within a 7.92-10.34 GHz working band of CPC (the RB is 26.5%). All in all, the proposed PC can realize the function switchover between LCPC and CPC, and the operating bands of the CPC can be shifted flexibly between the states 2 and 3. The proposed PC has great potential values in antennas, imaging systems, electromagnetic devices and so on.**

***Index Terms*— Cross-polarization conversion, linear-to-circular polarization conversion, solid-state plasma, tunability.**

I. Introduction

POLARIZATION converter (PC) is a kind of functional devices that can polarize the incident electromagnetic (EM) wave in the direction [1]. In general, due to the different impedance matching characteristics, the EM wave incidents on the surface of the object will produce two parts: reflection wave and transmission wave. Therefore, the PCs can be divided into the reflection PCs and transmission PCs. Because of the difference of phase and amplitude, the incident linear-polarized wave (PW) is invariably reflected into three categories which are cross-polarized wave, circular PW and elliptical PW, respectively, and it leads to three functions of reflective PCs (cross PC, linear-to-circular PC and linear-to-elliptical PC) [2]–[4]. Besides, the cross PC and linear-to-circular PC are not only widely utilized in the propagation of EM waves but also possessed a significant application value in the domain of nanometre photonic devices and antennas as well [5]–[7]. Up to this day, it is of common occurrence to explore various design schemes of PC already.

For the rapid development and widespread use of metamaterials, the bulky size problem of conventional PCs is gradually overcoming. Metamaterial, as an artificial composite periodic structure, possesses many extraordinary physical properties other than the natural materials [8]–[11], such as negative refractive index and negative dielectric constant. The regulation of equivalent dielectric constant and permeability can be achieved by designing the different resonators. At present, researchers have already implemented the polarization regulation of EM waves through metamaterials [12]–[14].

In recent years, a growing number of PCs have been proposed in succession. In 2016, a PC with a cross-shaped structure working at microwave band was designed by Zhang *et al.* [15], the cross-polarization conversion (CPC) can be implemented in the band of 8.1-13.8 GHz. However, its polarization conversion rate (PCR) is not high, reaching only about 80%. In 2017, a dual U-shaped PC was proposed by Mei *et al.* [16], which acquires a wider bandwidth of PCR (above 0.9) and better polarization conversion compared with the proposed PCs in Ref. [15]. However, most PCs can just achieve a single state or operate in a fixed band in such designs at present. In response to those shortages, Zeng *et al.* [17] designed a band-adjustable PC by using the solid-state plasma (SSP) in 2019. Thus, the operating band can be switched between 8.81-14.34 GHz and 14.34-19.61 GHz by exciting the bias voltage across the SSP resonators.

Generally speaking, the collective effect of charge carriers in solids is called the SSP effect [18]–[20]. For some specific materials, when the charge carrier concentration reaches a certain condition (the carrier concentration ranges from 10^{12} cm^{-3} to 10^{19} cm^{-3}) [21], it can express the characteristics of SSP. However, the carrier concentration can be adjusted by adding the bias voltage at both ends of the SSP resonators, and then the conversion between metallic and nonmetallic features of the resonance units can be realized [22]–[25].

Although the design of Zeng *et al.* [17] has realized the tunability of operating band preliminarily through the SSP, the conversion between functions has not been achieved. Hence, we propose a multi-function PC based on the SSP metasurface and three working states can be obtained by energizing different SSP resonators. When only the cross portion resonator located at the central area is activated (the state 1), the linear-to-circular polarization conversion can be obtained in 6.12-9.50 GHz with a relative bandwidth (RB)

Manuscript received December 23, 2019; revised February 12, 2020; accepted February 14, 2020. Date of publication February 19, 2020; date of current version February 26, 2020. This work was supported in part by the Open Research Program in China's State Key Laboratory of Millimeter Waves under Grant K201927 and in part by the Jiangsu Overseas Visiting Scholar Program for the University prominent Young and Middle-aged Teachers and Presidents. *(Corresponding author: Hai-Feng Zhang.)*

Yu-Peng Li, Tong Yang, Tang-Yi Sun, and Li Zeng are with the College of Electronic and Optical Engineering and College of Microelectronics, Nanjing University of Posts and Telecommunications, Nanjing 210023, China.

Hai-Feng Zhang is with the College of Electronic and Optical Engineering and College of Microelectronics, Nanjing University of Posts and Telecommunications, Nanjing 210023, China, and also with the State Key Laboratory of Millimeter Waves, Southeast University, Nanjing 210096, China (e-mail: hanlor@163.com).

Color versions of one or more of the figures in this article are available online at http://ieeexplore.ieee.org.

Digital Object Identifier 10.1109/JQE.2020.2975019

TABLE I
COMPARISON WITH OTHER REFLECTION POLARIZATION CONVERTERS

Reference	CPC	LCPC	Tunability
[26]	12.4 - 27.96 GHz	None	None
[27]	None	28 - 31.5 GHz	None
[28]	None	18.88 – 32.86 GHz 32.42 – 42.82 GHz	Band transfer
[29]	6.53 - 12.07 GHz	13.70 - 15.60 GHz	Function switching
Present study	State 2: 4.62 - 8.34 GHz State 3: 7.92 - 10.34 GHz	State 1: 6.12 - 9.50 GHz	Function switching Band transfer

of 43.3%. If all parts exclusive of the inner small arcs are excited (the state 2), the CPC can be performed with a RB of 57.4 %, which covers 4.62-8.34 GHz. The RB of state 3 which excites all parts exclusive of the outer big arcs is 25.6 %, whose operating band is 7.92-10.34 GHz. The proposed device fairly achieves two tunable modes of bandwidth transfer and function conversion.

Besides, more instances can be sought out to bear out the strong points of this project, and some of them are listed in Table.1. Most PCs in existence can perform one pattern of polarization conversion simply, such as references [26] and [27] which can implement CPC and LCPC within 12.40-27.96 GHz and 28.0-31.5 GHz respectively. Compared with above, PCs that can carry out the band shifting are more advantageous, as mentioned in [28], LPCP can be achieved in bands 18.88-32.86 GHz and 32.42-42.82 GHz by utilizing the gravity field technology. Besides, under one state, the design in [29] can realize CPC and LCPC in different bands. In a sense, this PC can realize the multi-function passively, but it cannot achieve the free regulation. However, compared to the above documentations with our present study again, it is lucid that the merits of our project are not only the function switching but also the band transfer. Based on what we knew, it is uncommon to achieve two types of switching and three states on one design, compared with the majority of PCs which possess single regulation means merely or no tunability, the utmost superiority of the proposed project is that the control means are diverse, so that it can adapt to more types of EM environment.

II. THEORETICAL MODEL

Fig.1 is a schematic diagram of the proposed PC which is based on the SSP metasurface. As displayed in Fig.1, the PC is composed of a top resonator layer and a bottom metal reflector, which is separated by a substrate layer in the middle. The bottom layer is a rectangular reflector of copper with the conductivity of 5.8×10^7S/m. The dielectric substrate on the second layer is F4B with a dielectric constant of 2.2 and a loss tangent of 0.0002. The top layer is made up of SSP units whose permittivity can be described by a Drude model $\varepsilon_p(\omega) = 12.4\omega_p/(\omega^2 + j\omega\omega_c)$ [30]. The related parameters of SSP are plasma frequency ω_p and the collision frequency ω_c, and the values of them are 2.9×10^{15} rad/s and 1.65×10^{11} 1/S,

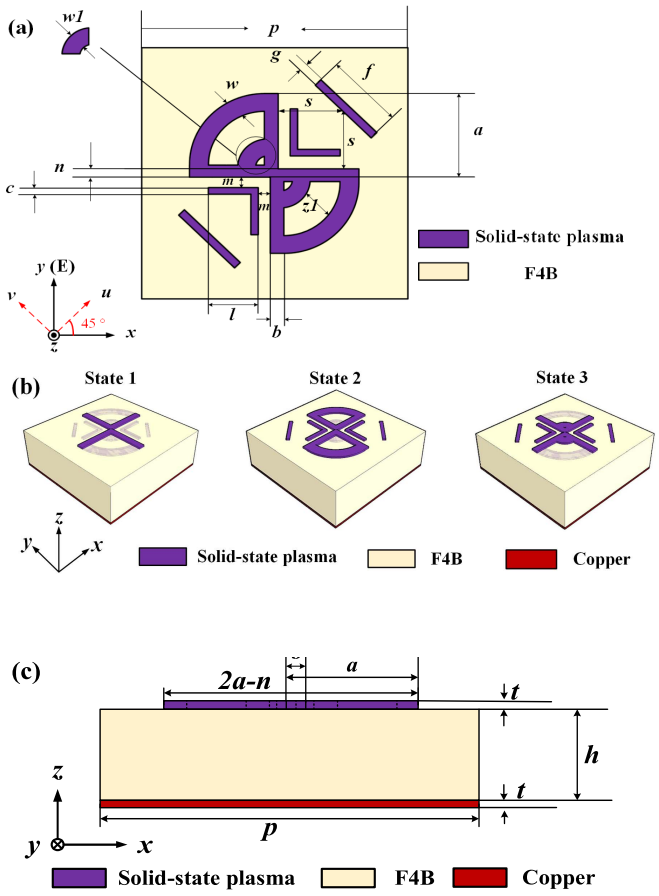

Fig. 1. Schematic diagrams of the proposed PC: (a) the front view of the unit cell, (b) the diagrammatic sketch in states 1 and 2, and (c) the side view of the unit cell.

respectively [30]. The resonators of the top layer take a couple of hollow sectors, a pair of L-shaped SSP patches and a couple of parallel SSP strips as the principal structure. The specific parameters and values for the proposed PC are given in Table.2. All the results are carried out under the commercial simulation software HFSS. The EM wave is incident to the PC along the z-axis perpendicularly. Besides, the direction of the electric field of EM wave is along the y-axis.

Utilizing the principle of SSP, we can attain three states by exciting different resonance units, the specific excitation circumstances are displayed in Fig.1(a). It is called the state 1 when merely the internal large cross unit is energized. However, based on the state 1, state 2 is a condition in which a pair of L-shaped patches, a couple of parallel strips and outer arcs are newly charged up, and the difference between the state 3 and state 2 is that the outer arcs are replaced by the inner arcs.

III. NUMERICAL RESULTS AND DISCUSSION

Generally, two indexes called the PCR and axial ratio (AR) are usually adopted to measure the quality of cross PC and linear-to-circular PC. The essence of polarization conversion is the conversion of electric field intensity in different directions,

TABLE II
THE PARAMETERS OF THE PROPOSED PC

Parameters	p	a	b	w	$w1$
Value (mm)	20	6.8	1	1.5	1.5
Parameters	t	s	n	m	$z1$
Value (mm)	0.03	5	0.2	1	4
Parameters	c	l	h	g	f
Value (mm)	0.5	4	6.4	0.7	5

and the PCR can reflect the characteristics of polarization conversion by calculating the reflection and transmission amplitudes, directly. For good performance, PCR should fit well to 1 when there is no absorption and diffraction, also, the part of PCR>0.9 is usually referred to as the working band in the industry. The formula for PCR is as follows [31]:

$$PCR = \frac{T_{yx}^2}{T_{yx}^2 + T_{xx}^2 + R_{yx}^2 + R_{xx}^2} \tag{1}$$

Furthermore, by combining amplitudes and phases, AR is a better choice to describe the performance of linear-to-circular PC. Normally, the operating band with AR<3 dB is called the portion with good polarization conversion. The specific calculation formula is as follows [32]:

$$AR = 10 \times \log_{10} \frac{(E_1 \cos\tau + E_2 \cos\varphi sin\tau)^2 + E_2^2 sin^2\varphi sin^2\tau}{(E_1 sin\tau + E_2 \cos\varphi \cos\tau)^2 - E_2^2 sin^2\varphi \cos^2\tau} \tag{2}$$

in which

$$\tau = \frac{1}{2}\arctan\left(\frac{2E_1E_2\cos\varphi}{E_1^2 - E_2^2}\right) \tag{3}$$

and

$$E_1 = S_{21}^{//},\ E_2 = S_{21}^{\perp} \tag{4}$$

The analysis of the state 1 is revealed in Fig.2. The reflection amplitude curves (red curves) and phase difference curve (blue curve) of PC are described by Fig.2(a) when the EM is incident vertically. In the operating band (6.12-9.50 GHz) of state 1, the reflection amplitude curves are mostly approached to each other while the phase difference is maintained at an odd number times of 90°. Thus, the conditions of linear-to-circular polarization conversion (LCPC) are satisfied. Also, it can be seen from Fig.2(a) that the value of AR is less than 0.3 in the frequency band of 6.12-9.50 GHz in the state 1, whose RB is 43.3%.

The schematic diagrams of PC in the latter two states are revealed in Fig.3. In Figs.3(a) and (b), the reflection amplitude curves of the states 2 and 3 are expressed by the red curves when the EM incidents along u-axis and v-axis, while the blue curves describe the reflection phase

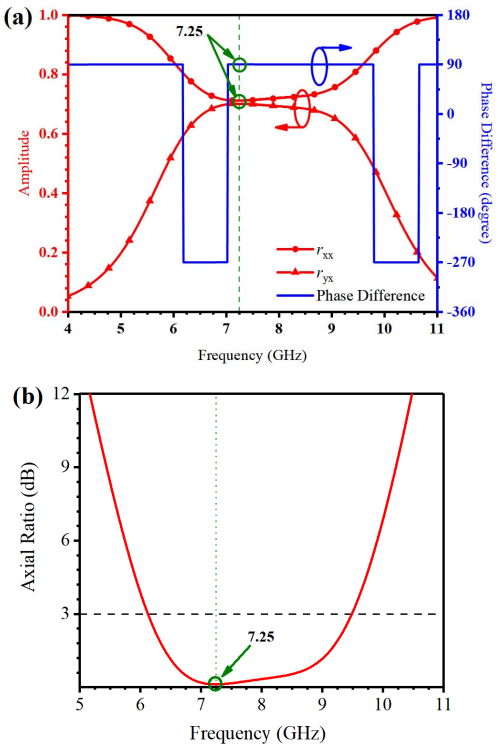

Fig. 2. Analysis of the state 1: (a) amplitude and phase difference curves of the state 1, and (b) AR curve of the state 1.

difference curves in this case. As we can see from the blue lines of Figs.3(a) and (b), the phase difference values of the states 2 and 3 are closed to 180 degrees in their respective operating bands, and the red curves are fitted to each other, which means that a 90° polarization rotation is well obtained. Two calculated PCR curves are spread in Fig.3(c) where the red solid line represents the states 2 with the operating band of 4.62-8.34 GHz and the blue dotted line denotes the state 3 with the band of 7.92-10.34 GHz. Obviously, the corresponding RBs of the sates 2 and 3 are 57.7%and 26.5%, respectively. The PCR of the two curves are stable above 0.9 in each band, which shows that the polarization conversion effect of PC is excellent in state 2 and state 3, respectively.

To better explain the principle of the proposed PC, the surface current diagrams of the SSP resonant units and the copper reflector are given in Fig.4. In the surface current diagrams of the SSP resonators, the red arrows indicate the main current direction. In the surface current diagrams of the copper reflector, the current direction is represented by the black arrows, whose components can be decomposed in the orthogonal direction of x-axis and y-axis by the different red arrows, respectively. The surface current diagrams of the state 1 at 7.25 GHz is exhibited in Fig.4(a), and the red currents 1 and 2 on the SSP resonant units are opposite to the red currents 1' and 2' on the copper reflector, which cause two circulating currents. Hence, the induced magnetic field $\mathbf{H}_1$ and $\mathbf{H}_2$ are formed by circulating currents (m_1 and m_2 represent the magnetic dipoles). Therefore, the electric field $\mathbf{E}$ is paralleled to the induced magnetic field $\mathbf{H}_1$ which leads to the emergence of polarization conversion. On the contrary,

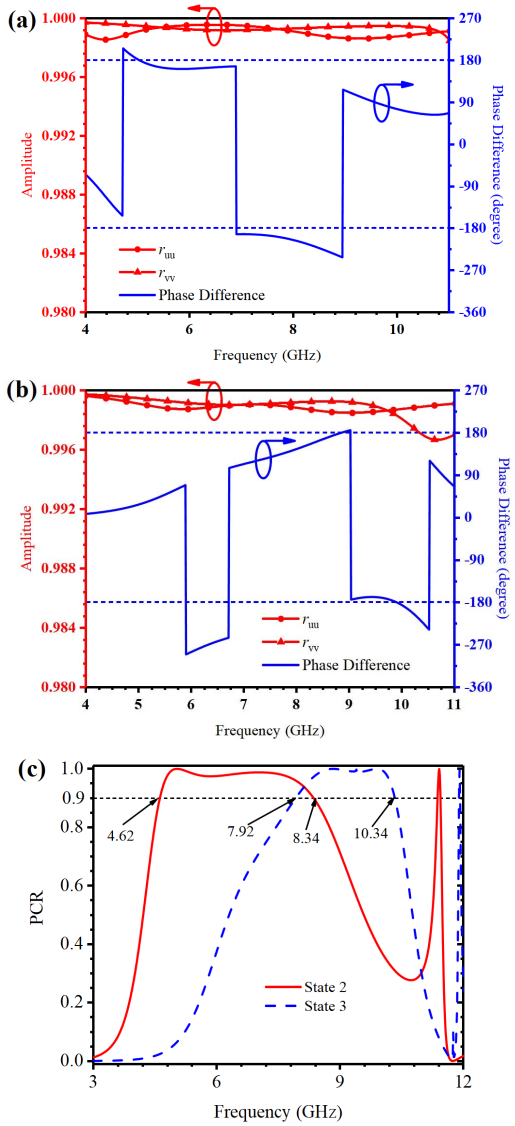

Fig. 3. Analysis of the states 2 and 3, (a) amplitude and phase difference curves of state 2, (b) amplitude and phase difference curves of state 2, and (c) the PCR curves of the states 1 and 2.

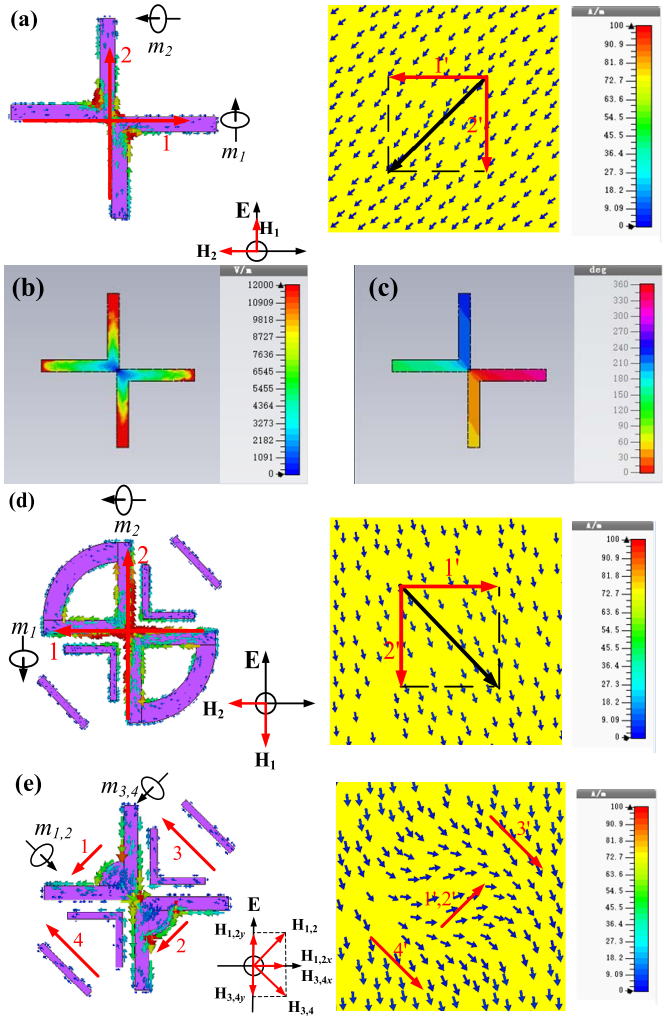

Fig. 4. The surface current diagrams, the electric field diagram and the phase spectrum of E of the SSP resonant units and the copper reflector, (a) the surface current diagrams at 7.25 GHz in the state 1, (b) the electric field diagram at 7.25 GHz in the state 1, (c) the phase spectrum of E at 7.25 GHz in the state 1, (d) the surface current diagrams at 4.80 GHz in the state 2, and (e) the surface current diagrams at 10.22 GHz in the state 3.

the electric field **E** is perpendicular to the induced magnetic field $\mathbf{H}_2$ and there is no polarization conversion generation. Furthermore, in the light of the principle of LCPC, a more in-depth analysis of state 1 at 7.25 GHz can be gained. Firstly, Fig.4(b) explicitly illustrates the point that the electric field of state 1 is concentrated at the four branches mainly. However, from the phase spectrum of each branch in Fig.4(c), it can be found out more clearly the phase of **E** takes four successive incremental steps of 90°, which leads to the clockwise rotation of the electric field vector of the reflected wave in space, and then the left-handed wave is formed. Combining Figs.2(a) and (b) again, it can be seen that an excellent effect of LCPC conversion can also be confirmed at 7.25 GHz, where two amplitude curves are the closest to each other (marked by the green circle in Fig.2). According to the phase difference ($\Delta\varphi = \varphi_{yx}$-$\varphi_{xx}$) is +90 °, the emitted light can be regarded as a left-handed circularly polarized wave. This conclusion coincides with the result discussed above.

The surface current diagrams of the state 2 at 4.80 GHz is similar to those mentioned above, so the similar description does not need to repeat. However, the particular note is the current distribution of state 3 at 10.22 GHz. As revealed in Fig.4(e), two main mutually orthogonal currents have emerged on the SSP resonant units (the currents 1, 2 and the currents 3, 4) which are opposite to the currents 1', 2' and 3', 4' on the copper reflector, severally. The upper and lower currents correspond mutually to form circular currents, which create the induced magnetic fields $\mathbf{H}_{1,2}$ and $\mathbf{H}_{3,4}$($m_{1,2}$ and $m_{3,4}$ represent the magnetic dipoles). Nevertheless, the induced magnetic fields can be disassembled into the x-axis ($\mathbf{H}_{1,2x}$ and $\mathbf{H}_{3,4x}$) and y-axis ($\mathbf{H}_{1,2y}$ and $\mathbf{H}_{3,4y}$) components. Thus, the reason why there is polarization conversion in the y-axis is that the components of the induced magnetic fields in the y-axis are parallel to the electric field **E**, and the components of the induced magnetic fields in the x-axis are in contrast.

Based on those three states, the effects of diverse incidence angles (IA) on the AR or PCR in different states are plotted

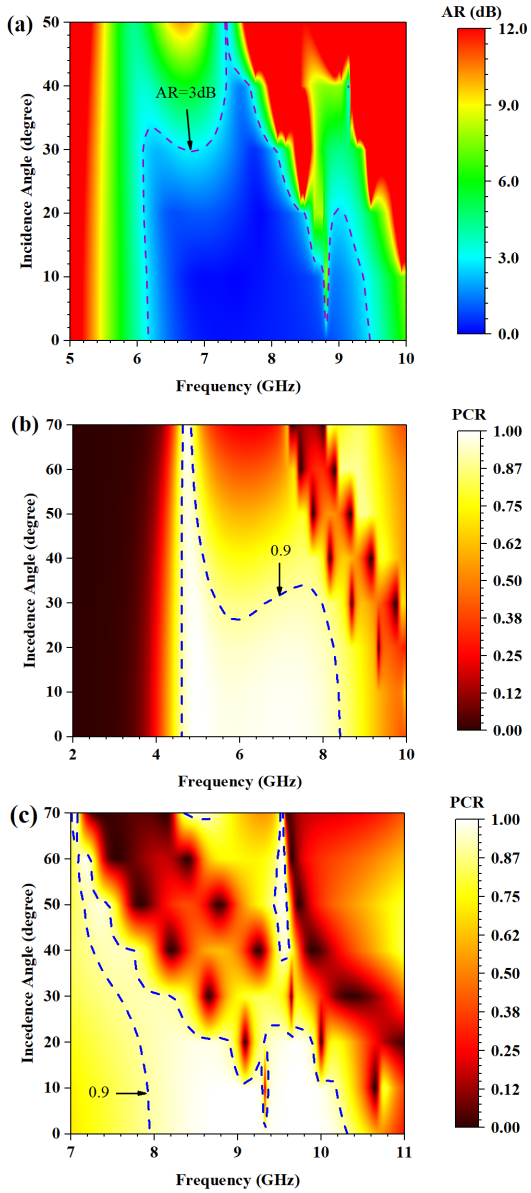

Fig. 5. The spectra of AR and PCR with diverse incidence angles in the different states: (a) the AR spectra of the presented PC in the state 1 when the IA varies from 0° to 50°, (b) the PCR spectra of the proposed PC in the state 2 when the IA runs from 0° to 70°, and (c) the PCR spectra of the given PC in the state 3 when the IA spans from 0 ° to 70°.

in Fig.5, respectively. The variation of the AR in the state 1 with the IA enlarged from 0 to 50 degrees is depicted by Fig.5(a). It can be seen from Fig.5(a) that there will be a deteriorated frequency point at the higher frequencies, whose range will expand with the increase of the value of IA and move to the intermediate frequency region. Besides, the AR of intermediate band ascends with the rise of the IA. Figs.5(b) and (c) show the change spectra of PCR when the IA ranges from 0 to 70 degrees, where the contour line of PCR=0.9 is depicted by the blue dashed lines. From Fig.5(b), we can pick up the information that the operating band keeps stable when the IA increases from 0 to 25 degrees in the state 2. With the enhancement of the IA, the band shrinks sharply,

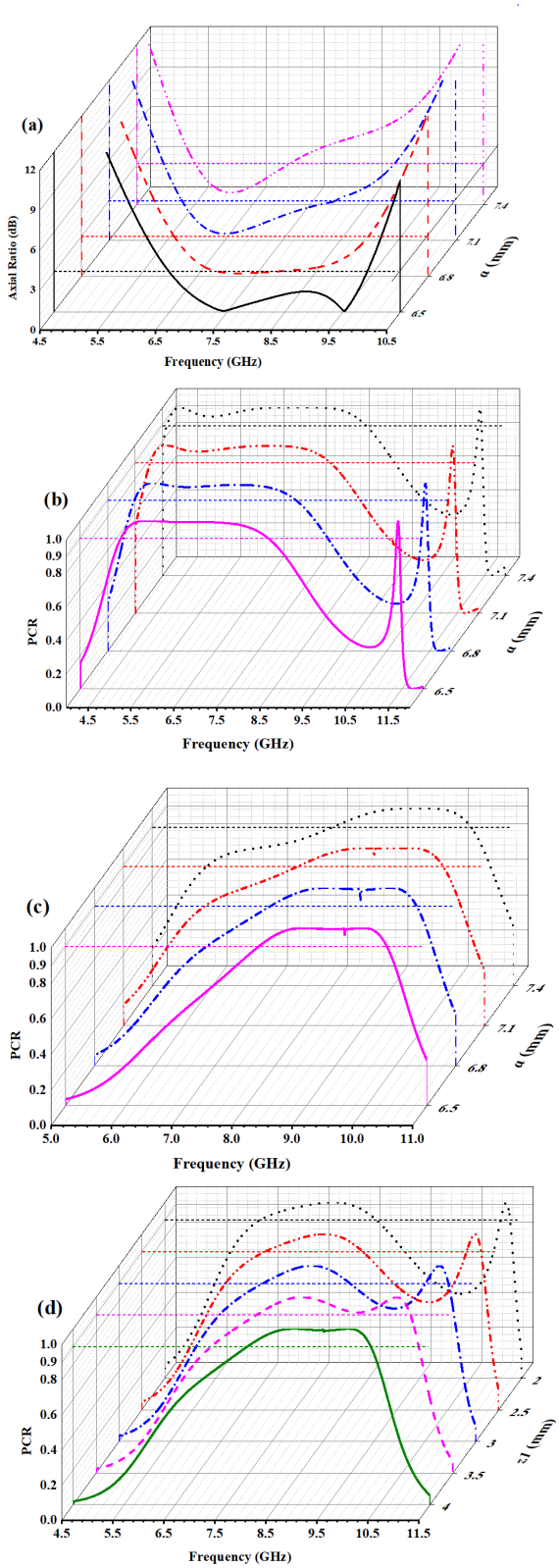

Fig. 6. The curves of AR and PCR when other parameters remain invariant but only parameters a and $z1$ are changed, (a) the AR curves of the state 1 when a = 6.5 mm, 6.8 mm, 7.1 mm and 7.4 mm, respectively, (b) the PCR curves of the state 2 when a = 6.5 mm, 6.8 mm, 7.1 mm and 7.4 mm, respectively, (c) the PCR curves of the state 3 when a = 6.5 mm, 6.8 mm, 7.1 mm and 7.4 mm, respectively, and (d) the curves of PCR for the sate 3 when $z1$ = 2 mm, 2.5 mm, 3 mm, 3.5 mm and 4 mm, respectively.

and it concentrates on the lower frequencies ultimately. Next, through the analysis of Fig.5(c) which describes in the state 3, we can conclude that there will be a worsen point at 9.2 GHz to divide the operating band into two portions, and with the enlargement of the IA, the scope of deterioration is expanding. In succession, the working band is narrowing down and shifted toward the lower frequency band when the IA is larger than 25 degrees.

The influence of structural parameters *a* and *z1* on the AR and PCR will be gone a step further to discuss. Among them, Figs.6(a), (b) and (c) depict the influence of parameter *a* on three states. In the state 1, the curves of AR vs. *a* which increase in number with an identical span are described by Fig.6(a), and one can see from it that AR can be lifted by the raise of *a* at higher frequencies. When the value of parameter *a* varies from 6.5 mm to 7.4 mm, the operating band of AR$<$3 dB also diverts from 6.51-9.91 GHz to 5.23-7.11 GHz. However, the raise of parameter *a* enlarges the bandwidth of state 2 (the RB changed from 50.50 % to 71.45 %), meanwhile, the PCR is also abated at the lower frequencies, slightly. For the state 3, with the enlargement of parameter *a*, the PCR at the lower frequencies is elevated gradually but not significantly. So, it is an undeniable fact that the transformation of a possessed seldom effect on the band range of PCR$>$0.9. Take into account what we have discussed above, we may safely conclude that $a = 6.8$ mm is the optimal value at present through considering the bandwidth and the indexes quality of three states. After *a* is determined, it is the turn for parameter *z1* to be included in our discussion. The parameter *z1* is expressed the distance between the inner ring and the outer ring, and we only need to take the effects on the state 3 into discussion. For the state 3, *z1* primarily affects the PCR in intermediate frequency and higher frequency regions. In the wake of the increase of *z1*, the two parts gradually approach each other, and a complete continuous operating band of 7.92-10.34 GHz is formed, ultimately. In consideration of high conversion efficiency and the connectivity of bandwidth in two states, *z1*=4 mm is considered to be the most appropriate parameter value at present.

IV. Conclusion

To sum up, a multifunctional PC based on the SSP metasurface is presented in this paper. The proposed PC has three operating states. In the state 1, the LCPC can be realized in the frequency region of 6.12-9.50 GHz, whose RB is 43.3%. In the states 2 and 3, the CPC can be obtained, and their operating bands span from 4.62 to 8.34 GHz. and from 7.92 to 10.34 GHz, and the corresponding RBs are 57.7% and 26.5%, respectively. Switching three working states can be realized by exciting the different SSP resonators, thereby the functional conversion and operating band shifting are implemented.

References

[1] L. Martinez-Lopez, J. Rodriguez-Cuevas, J. I. Martinez-Lopez, and A. E. Martynyuk, "A multilayer circular polarizer based on bisected split-ring frequency selective surfaces," *IEEE Antennas Wireless Propag. Lett.*, vol. 13, pp. 153–156, 2014.

[2] Z. Li, W. Liu, H. Cheng, S. Chen, and J. Tian, "Realizing broadband and invertible Linear-to-circular polarization converter with ultrathin single-layer metasurface," *Sci. Rep.*, vol. 5, no. 1, p. 18106, Dec. 2015.

[3] B. Lin, J.-L. Wu, X.-Y. Da, W. Li, and J.-J. Ma, "A linear-to-circular polarization converter based on a second-order band-pass frequency selective surface," *Appl. Phys. A, Solids Surf.*, vol. 123, no. 1, p. 43, Dec. 2016.

[4] Y. Jiang, L. Wang, J. Wang, C. N. Akwuruoha, and W. Cao, "Ultra-wideband high-efficiency reflective linear-to-circular polarization converter based on metasurface at terahertz frequencies," *Opt. Express*, vol. 25, no. 22, p. 27616, Oct. 2017.

[5] Y.-J. Chiang and T.-J. Yen, "A composite-metamaterial-based terahertz-wave polarization rotator with an ultrathin thickness, an excellent conversion ratio, and enhanced transmission," *Appl. Phys. Lett.*, vol. 102, no. 1, Jan. 2013, Art. no. 011129.

[6] D. L. Markovich, A. Andryieuski, M. Zalkovskij, R. Malureanu, and A. V. Lavrinenko, "Metamaterial polarization converter analysis: Limits of performance," *Appl. Phys. B, Lasers Opt.*, vol. 112, no. 2, pp. 143–152, Mar. 2013.

[7] Y.-J. Chiang, C.-S. Yang, Y.-H. Yang, C.-L. Pan, and T.-J. Yen, "An ultrabroad terahertz bandpass filter based on multiple-resonance excitation of a composite metamaterial," *Appl. Phys. Lett.*, vol. 99, no. 19, Nov. 2011, Art. no. 191909.

[8] J. Hao *et al.*, "Manipulating electromagnetic wave polarizations by anisotropic metamaterials," *Phys. Rev. Lett.*, vol. 99, no. 6, Aug. 2007, Art. no. 063908.

[9] N. K. Grady *et al.*, "Terahertz metamaterials for linear polarization conversion and anomalous refraction," *Science*, vol. 340, no. 6138, pp. 1304–1307, May 2013.

[10] K. Aydin, Z. Li, L. Sahin, and E. Ozbay, "Negative phase advance in polarization independent, multi-layer negative-index metamaterials," *Opt. Express*, vol. 16, no. 12, pp. 8835–8844, Jun. 2008.

[11] I. A. I. Al-Naib, C. Jansen, N. Born, and M. Koch, "Polarization and angle independent terahertz metamaterials with high Q-factors," *Appl. Phys. Lett.*, vol. 98, no. 9, Feb. 2011, Art. no. 091107.

[12] X.-J. He *et al.*, "Broadband and polarization-insensitive terahertz absorber based on multilayer metamaterials," *Opt. Commun.*, vol. 340, pp. 44–49, Apr. 2015.

[13] X. Jing, X. C. Gui, P. W. Zhou, and Z. Hong, "Physical explanation of Fabry–Pérot cavity for broadband bilayer metamaterials polarization converter," *J. Lightw. Technol.*, vol. 36, no. 12, pp. 2322–2327, Jun. 15, 2018.

[14] J.-X. Zhao, B.-X. Xiao, X.-J. Huang, and Y.-H. Lin, "Multiple-band reflective polarization converter based on complementary L-shaped metamaterial," *Microw. Opt. Technol. Lett.*, vol. 57, no. 4, pp. 978–983, Apr. 2015.

[15] L. Zhang, P. Zhou, H. Lu, L. Zhang, J. Xie, and L. Deng, "Realization of broadband reflective polarization converter using asymmetric cross-shaped resonator," *Opt. Mater. Express*, vol. 6, no. 4, pp. 1393–1404, Mar. 2016.

[16] Z. L. Mei, X. M. Ma, C. Lu, and Y. D. Zhao, "High-efficiency and wide-bandwidth linear polarization converter based on double U-shaped metasurface," *AIP Adv.*, vol. 7, no. 12, 2017, Art. no. 125323.

[17] L. Zeng, H.-F. Zhang, G.-B. Liu, and T. Huang, "Broadband Linear-to-Circular polarization conversion realized by the solid state plasma metasurface," *Plasmonics*, vol. 14, no. 6, pp. 1679–1685, May 2019.

[18] R. Hirota and K. Suzuki, "Propagation of waves in a bounded solid state plasma in transverse magnetic fields," *J. Phys. Soc. Jpn.*, vol. 21, no. 6, pp. 1112–1118, Jun. 1966.

[19] H. J. Kuno and W. D. Hershberger, "Microwave faraday effect and propagation in a circular solid-state plasma waveguide," *IEEE Trans. Microw. Theory Techn.*, vol. 15, no. 12, pp. 661–668, Dec. 1967.

[20] A. A. Bokrinskaia and G. P. Krasilich, "Characteristics of the interaction of orthogonal inductance coils coupled by a bounded solid-state plasma," *Radioehlektronika*, vol. 18, pp. 102–105, Jan. 1975.

[21] X.-K. Kong, J.-J. Mo, Z.-Y. Yu, W. Shi, H.-M. Li, and B.-R. Bian, "Reconfigurable designs for electromagnetically induced transparency in solid state plasma metamaterials with multiple transmission windows," *Int. J. Mod. Phys. B*, vol. 30, no. 14, Jun. 2016, Art. no. 1650070.

[22] B. Luo, J. W. Johnson, F. Ren, K. W. Baik, and S. J. Pearton, "Effect of plasma enhanced chemical vapor deposition of SiNx on n-GaN Schottky rectifiers," *Solid-State Electron.*, vol. 46, no. 5, pp. 705–710, May 2002.

[23] M. Tang, L. J. Sperling, D. A. Berthold, A. E. Nesbitt, R. B. Gennis, and C. M. Rienstra, "Solid-state NMR study of the charge-transfer complex between Ubiquinone-8 and disulfide bond generating membrane protein DsbB," *J. Amer. Chem. Soc.*, vol. 133, no. 12, pp. 4359–4366, Mar. 2011.

[24] N. J. Morgenstern Horing and M. M. Yildiz, "Quantum theory of longitudinal dielectric response properties of a two-dimensional plasma in a magnetic field," *Ann. Phys.*, vol. 97, no. 1, pp. 216–241, Mar. 1976.
[25] P. E. M. P. J. Gaudreau, J. A. Casey, M. A. Kempkes, T. J. Hawkey, and J. M. Mulvaney, "Solid-state modulators for plasma immersion ion implantation applications," *J. Vac. Sci. Technol. B, Microelectron. Nanometer Struct.*, vol. 17, no. 2, p. 888, 1999.
[26] X. Gao, X. Han, W. P. Cao, H. O. Li, H. F. Ma, and T. J. Cui, "Ultra-wideband and high-effificiency linear polarization converter based on double V-shaped metasurface," *IEEE Trans Antennas Propag.*, vol. 63, no. 8, pp. 3522–3530, Aug. 2015.
[27] M. Akbari, M. Farahani, A.-R. Sebak, and T. A. Denidni, "Ka-band linear to circular polarization converter based on multilayer slab with broadband performance," *IEEE Access*, vol. 5, pp. 17927–17937, 2017.
[28] L. Zeng, H.-F. Zhang, G.-B. Liu, and T. Huang, "A three-dimensional Linear-to-Circular polarization converter tailored by the gravity field," *Plasmonics*, vol. 14, no. 6, pp. 1347–1355, Mar. 2019.
[29] Q. Zheng, C. Guo, and J. Ding, "Wideband metasurface-based reflective polarization converter for Linear-to-Linear and Linear-to-Circular polarization conversion," *IEEE Antennas Wireless Propag. Lett.*, vol. 17, no. 8, pp. 1459–1463, Aug. 2018.
[30] H.-F. Zhang, H. Zhang, Y. Yao, J. Yang, and J.-X. Liu, "A band enhanced plasma metamaterial absorber based on triangular ring-shaped resonators," *IEEE Photon. J.*, vol. 10, no. 4, pp. 1–10, Aug. 2018.
[31] H. Su *et al.*, "Terahertz multi-band reflective polarization converter based on TSRR metamaterial," in *Proc. 11th Int. Symp. Antennas, Propag. EM Theory (ISAPE)*, Oct. 2016, pp. 206–209.
[32] X. Ma, C. Huang, M. Pu, C. Hu, Q. Feng, and X. Luo, "Single-layer circular polarizer using metamaterial and its application in antenna," *Microw. Opt. Technol. Lett.*, vol. 54, no. 7, pp. 1770–1774, Apr. 2012.

Yu-Peng Li was born in Guizhou, China, in 1999. She is currently pursuing the degree with the Nanjing University of Posts and Telecommunications, Nanjing, China. Her main research interests include polarization converters and tunable metamaterials.

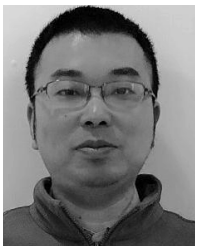

Hai-Feng Zhang was born in Jiangxi, China, in 1978. He received the M.Sc. degree in electronics science and technology from Nanchang University, Nanchang, China, in 2008, and the Ph.D. degree from the College of Electronic and Information Engineering, Nanjing University of Aeronautics and Astronautics, Nanjing, in 2014.

He is currently working as a Professor with the College of Electronic and Optical Engineering and College of Microelectronics, Nanjing University of Posts and Telecommunications, Nanjing. His main research interests include the computational electromagnetics, plasma photonic crystal, plasma stealthy, and electromagnetic properties of metamaterials.

Tong Yang was born in Heilongjiang, China, in 1999. She is currently pursuing the degree with the Nanjing University of Posts and Telecommunications, Nanjing, China. Her main research interests include absorbers and tunable metamaterials.

Tang-Yi Sun was born in Jiangsu, China, in 1999. He is currently pursuing the degree with the Nanjing University of Posts and Telecommunications, Nanjing, China. His main research interests include polarization rotators and absorber based on metasurfaces.

Li Zeng was born in Hunan, China, in 1999. He is currently pursuing the degree with the College of Electronic and Optical Engineering and College of Microelectronics, Nanjing University of Posts and Telecommunications, Nanjing, China. His main research interests include the tunable polarization converter and ultra-broadband absorber.